RESEARCH ARTICLE

SPE INSPIRING PLASTICS PROFESSIONALS | Polymer COMPOSITES | **WILEY**

A novel strategical approach to mitigate low velocity impact damage in composite laminates

L. Amorim | A. Santos | J. P. Nunes | G. Dias | J. C. Viana

IPC—Institute for Polymers and Composites, University of Minho, Guimarães, Portugal

Correspondence
L. Amorim, IPC—Institute for Polymers and Composites, University of Minho, Guimarães, Portugal.
Email: luis.amorim@dep.uminho.pt

Abstract

This paper describes a new interleaving methodology to improve composite laminates' low velocity impact (LVI) damage resistance. The approach relies on analyzing interlaminar stress in a conventional aircraft laminate to determine the appropriate interleaving strategy. A model was built to identify the larges interlaminar stress, and two interleaving strategies were defined, normal and shear stress. Four thin interleaving veils were used to validate strategies. Non- and interleaved laminates were submitted to LVI tests at 13.5, 25 and 40 (J) of energy. Despite interleaved laminates revealed an increase in thickness and resin volume fraction compared to the reference, they were limited to 10% and 7.6% on shear stress interleaved layups. Interleaved laminates also demonstrated an improved external and internal LVI damage resistance, especially when shear stress interleaving strategy was adopted, preventing external damage and mitigating internal damage up to 59%. No correlation between the veil's type and impact damage demonstrates the importance of interleaving strategies over the veil's characteristics.

Highlights

- Simplified quasi-static elastic Abaqus model identified the largest in-plane normal (axial and transversal) and shear interlaminar stresses;
- Four thin veils were used to validate interleaving strategies adopted;
- All laminates were produced using the same conditions to minimize process influence on experimental tests;
- Under low velocity impact (LVI) tests, interleaving laminates in the largest shear stress interlaminar can prevent external damage and mitigate internal damage up to 59%, comparing to the reference;
- No correlation between the veils and damage demonstrates the relevance of the interleaving strategy over the veil type.

KEYWORDS

composites, damage resistance, finite element analysis (FEA), low velocity impact (LVI), strategic interleaving

1 | INTRODUCTION

High-demanding applications, such as aeronautic, aerospace, sports and defense, have been taking advantage of high in-plane mechanical performance (e.g., stiffness and strength) and low-density of laminate fiber reinforced polymer (FRP) composite materials to enhance performance.[1–3] However, materials' high brittleness and layer-by-layer architecture make them quite vulnerable to out-of-plane loading.[4] Under these conditions, composite laminates tend to develop internal barely visible damages that may propagate throughout the interlaminar region, also known as delaminations, leading to a catastrophic and unpredictable failure of the composite part.[2,5–8]

To improve composites' toughness, composite design engineers have proposed different numerical and experimental approaches to address such goals, such as the insertion of through-the-thickness mechanical reinforcements,[9–11] matrix[12–14] and/or fibers surface[15,16] modification, or the inclusion of toughening systems into the interlaminar resin rich regions of laminates, so-called interleaving approach.[17,18] This last method has been shown to be very effective in improving interlaminar fracture toughness (mode I and II) and impact damage resistance and tolerance in composites by delaying interlaminar crack propagation.[17–22] In addition, this technique can also provide composites with multifunctionalities, besides being cheap and easy to implement in current manufacturing processes. Since the beginning, a wide range of interlaminar toughening systems have been proposed from "high-strain" resins, polymeric films and shape memory alloy (SMA) to nanoparticles or thin and nano fibrous veils.[18,23–29] Nevertheless, using films has revealed challenges to achieving complete impregnation in liquid resin manufacturing composite processes,[25] thus, more porous toughening systems have been considered. Carbon nanotubes (CNTs), whether sprayed, grifted or embedded in electrospun fibers, have improved the interlaminar damage resistance of laminate composites. This is mainly attributed to the addition of interfacial bonding and toughening mechanisms, such as CNT bridging and pull-out, that they can provide to those resin-rich regions due to their nano-dimensions and high aspect ratio, which provides high the specific area available to be in contact with the resin, compared, for instance, with convent fibrous veils. In addition, their typically low concentration in interlaminar regions do not compromise fiber dominate properties, such as in-plane stiffness or strength. In resin transfer manufacturing processes, such nano interlaminar toughening systems may minimize issues associated with permeability. On the other hand, the need for functionalisation to improve adhesion and ensure a good distribution over the interlaminar region are some limitations to their piratical implementation in industrial processes.[18,26,27,30–34] Micro fibers in veil form or just dispersed over the interlaminar region have also improved composites' damage resistance and tolerance. Those enhancements were mainly attributed to the network microstructure (coverage), while the material of the fibers did not significantly influence damage response.[18,19,35] Nanofibrous veils can offer superior mechanical properties and larger bonding surface areas (specific surface area) between fibers and matrix. However, when compared to micro veils, only modest improvements are observed in interlaminar fracture toughness above certain coverage value. This suggests that their higher coverage reduces permeability, making them to behave more like a film.[18]

Some studies have also focused on the suitability of interleaving techniques to improve LVI damage resistance and tolerance.[19–22,35–39] García-Rodríguez et al.[19] interleaved two types of coPA veils, with identical areal weights and different melting temperatures, between each ply of a quasi-isotropic laminate. They observed that veils that have melted during the composites manufacturing process have reduced LVI damage and enhanced residual strength in CAI tests. Chen et al.[21] have used short polyimide (PI) fiber nets with different areal weights as CFRP interleaving structures. Under LVI conditions, veils with areal weight equal to or above 20 g/m^2 have improved peak-load and less severe damages on interleaved laminates compared to the non-interleaved reference. Jefferson et al.[40] proposed hybrid multiphase laminate architectures to improve LVI damage resistance and tolerance. Two configurations were studied, intercalate and sandwich layups, where chopped glass fibers were interleaved and sandwiched, respectively, by a plain weave glass fiber. The results demonstrated that the layup configuration significantly affects LVI and tensile after impact (TAI) composite performance. The sandwich laminate showed better impact properties and damage tolerance, while the intercalate layup demonstrated better LVI damage resistance due to its ability to redistribute the damage more effectively.

Despite the promising results claimed by the authors, in many cases, this approach revealed a negative effect on in-plane mechanical properties, reducing tensile, flexural and compression properties.[37] Such a phenomenon is attributed to reduced fiber volume fraction and increased thickness of interlaminar toughened region.[22] Complementary to this, other studies suggest that thinner interleaved layers may mitigate the adverse effect on in-plane properties since the intra-ply shear resistance of the interlaminar toughening layer is increased.[41,42]

Given the benefits of the interleaving technique for LVI damage resistance in composite laminates, it is of paramount importance to optimize the design of interleaved

composites by identifying the interlaminar regions susceptible to delamination and avoiding excessive interleaving which leads to increased thickness and reduced fiber volume fraction. A few works can be found in the literature aiming at a selective interleaving approach.[38,39,43] Yi and An[43] spread a toughening agent, amorphous polyether ketone with phenolphthalein group (PEK-C), into a quasi-isotropic laminate using different interleaving sequences. They concluded that the interleaving arrangement influences the impact damage and residual strength after impact. Saghafi et al.[38] used cohesive zone modeling to identify the optimal interleaving location in thin and thick quasi-isotropic composite laminates. Simulation results indicated top layers as the best interleaving location for thick laminates to reduce impact damage, while mid layers are optimal for thin composites. Ramji et al.[39] studied the influence of interleaf distribution of polyphenylene sulfide (PPS) veil into a bidirectional carbon/epoxy laminate. They observed that interleaving configuration could modify the mechanical impact response of the laminate after delamination onset load. Specifically, the laminates with the higher number of interleaved veils and interleaved in the mid layers had reduced damage. Despite the promising results obtained by selective interleaving regarding low velocity damage, none of the studies cited above mentioned its impact on in-plane mechanical properties nor any alternative strategy mitigation of its possible adverse effect. In this context, numerical simulations can be essential in the selective interleaving approach. They can identify critical internal stresses through the thickness of the laminate, predict the micro- and macro-scale interactions between the different material systems and interfaces, or even optimize the structural design of the toughening layer, as currently is done in other composite structures.[44–48]

According to Choi and Chang,[49] when an impact occurs, minor damages such as matrix cracking initially occur at the intralaminar level due to shear stresses. These damages then spread up to the interlaminar region due to bending stresses and propagate throughout the resin-rich regions. This causes critical damages such as fiber breakage or delaminations, which can result in the composite part failing catastrophically.

Assuming that the interleaving method mainly prevents damage propagation in interlaminar regions, in this work, we propose a new methodology for selective interleaving to improve the LVI damage resistance of laminated composites and minimize thickness increment and fiber volume fraction reduction. The herein proposed approach relies on a preliminary study of interlaminar stresses in the design stage of the composite project that will determine the appropriate interleaving strategy. In light of this, a simplified finite elements (FE) elastic model was developed to identify the most significant in-plane normal (both axial and transversal) and shear stress mismatches between two adjacent plies in a conventional aircraft carbon/epoxy laminate (LS), which theoretically should pinpoint the regions where damages are most likely to propagate. Afterwards, both strategical interleaving approaches were evaluated and compared to the non-interleaved reference laminate. Four thin veils made from glass, carbon, aramid and polyester fibers were used as interlaminar toughening systems to validate the proposed strategies. Each veil microstructural network was characterized prior to laminates' production under similar conditions of vacuum bag infusion. Finally, LVI mechanical response and damage resistance of interleaved configurations were compared with a non-interleaved reference layup.

2 | EXPERIMENTAL

2.1 | Materials

The laminates were produced using Angeloni's Dynanotex HS 24/150 DLN2 150 g/m^2 unidirectional carbon fiber (UDCF). The matrix system was a low viscosity bicomponent epoxy resin from Sika®. A 7:3 ratio of CR83 neat resin and CH83-6 hardener were mixed. For interleaving, ACP Composites provided four thin non-woven fibrous veils made of glass (17 g/m^2), carbon (17 g/m^2), aramid (14 g/m^2), and polyester (17 g/m^2).

The fibrous network of each veil was analyzed to assess its coverage. Ten samples of each veil were inspected under transmission magnifier (Olympus SZ-PT) and their coverage was determined by using the Leica Application Suite (LAS v4.4.) image analysis software. The theoretic contact area between fibers and matrix, specific surface area (Sf), and the fibers' cross-section of each veil were evaluated under a scanning electron microscope (SEM). Details about Sf determination can be consulted in Data S1, Part A.

2.2 | Laminates

Laminates were vacuum bag infused under identical conditions. UDCF tissues and veils were laser-cut, stacked manually, and vacuum-bagged onto a flat glass mold. Before infusion, the resin and hardener mixture were degassed in a vacuum chamber for 20 min to remove air bubbles. Resin infusion was performed at room temperature, and left to cure for 48 h, before a post-curing process at 70°C for 8 h.

This work used a standard aircraft laminate (LS) as a study case. Thus, interleaved and non-interleaved

TABLE 1 Laminates' layup.

| Laminate | Interleaving location | Layers | | Stacking sequence |
		UDCF tissue	Veil	
LS	Non-interleaved	28	-	$[0/45/90/−45/45/−45/0/0/−45/45/−45/90/45/0]_S$
Interleaved laminates	Normal stress	28	6	$[0/V/45/V/90/V/−45/45/−45/0/0/−45/45/−45/90/45/0]_S$
	Shear stress	28	6	$[0/V/45/90/−45/V/45/V/−45/0/0/−45/45/−45/90/45/0]_S$

Note: V interleaf veil.

(reference) laminates were produced using the same base UDCF layup. The proposed interleaving strategy aims at a selective interlaminar region modification using thin commercial veils, thereby minimizing thickness incrementation and fiber volume fraction reduction. A simplified FEA mesoscale quasi-static indentation model was first conducted to identify the most significant in-plane normal and shear stress mismatch between adjacent plies of LS laminate. From the results, two sets of only six interfaces (in a total of 27 interfaces), were identify and interleaved by the veils. These interfaces, corresponding to normal and shear stresses, identified from now on as critical normal and shear stresses, respectively, were interleaved by the four types of veils mentioned above. More details about the FE model are discussed later in Section 3. All layups, namely, non- and interleaved laminates, are presented in Table 1.

The thickness of the laminates was evaluated by measuring all LVI specimens of each configuration in four different places using a caliper rule. Four small samples were randomly taken from each laminate to examine its cross-section. All samples were embedded in resin using a silicone mold, finely polished, and covered with a thin layer of gold before being observed under SEM.

Laminates' carbon fibers, resin and veils volume fractions were also determined. The procedure used to determine them is described in detail in Data S1, Part B.

2.3 | Drop-weight low velocity impact tests

The LVI tests were conducted using Ceast's "Fractovis Plus" drop-weight impact testing machine equipped with an anti-rebounding system. The machine used a 20 mm diameter piezoelectric hemispherical steel strike impactor weighing 5.045 Kg for the entire testing campaign.

The primary goal of this study is to assess the effectiveness of interleaving techniques in reducing the impact of Barely Visible Impact Damage (BVID) on composite laminates. In light of this, initial LVI tests on LS laminates limited impact energy to a maximum of 40 J, ensuring that no perforation occurs. So, three impact energy levels, namely 13.5, 25 and 40 J, were selected. To ensure the desired impact energy, the distance between the impactor tip and the impact surface was carefully adjusted. Specimens measuring 150 mm × 100 (mm), according to ASTM D7136/D7136M standard, were clamped to a plate with four rubber tips. Three interleaved and four non-interleaved specimens were tested for each energy level.

Samples were visually inspected after impact for back-face damage analysis and measured with a caliper rule to evaluate their maximum diametral extent. Ria Blades.SA conducted ultrasonic inspections before and after impact tests using 1 MHz Olympus—Omni Scan Sx C-scan equipment to evaluate internal damages induced.

3 | FE MODEL

A preliminary study was conducted to determine the strategic placement of thin veils between layers of LS laminate. This study examined the distribution of normal (axial and transverse) and shear stress at interlaminar regions across the thickness of reference laminate under bending conditions.

Some studies have reported similarities between LVI and quasi-static indentation tests.[50,51] Using ABAQUS® FEM software, a simple quasi-static elastic FE analysis was used to evaluate interlaminar stresses in the indentation region under the elastic regime. The simulation of the LVI experimental tests involved modeling the simply supported impact specimen and the indenter with the exact same geometry. The specimen was modeled as an elastic solid using conventional linear cubic C3D8R elements where elastic orthotropic properties were set lamina by lamina. The indenter was modeled as a discrete rigid part. A mesh convergence study was conducted to ensure an accurate representation of the test during elastic deformation for a maximum displacement of 2.5 mm. The study revealed an error of approximately 5% in the loading force obtained compared to the experimental
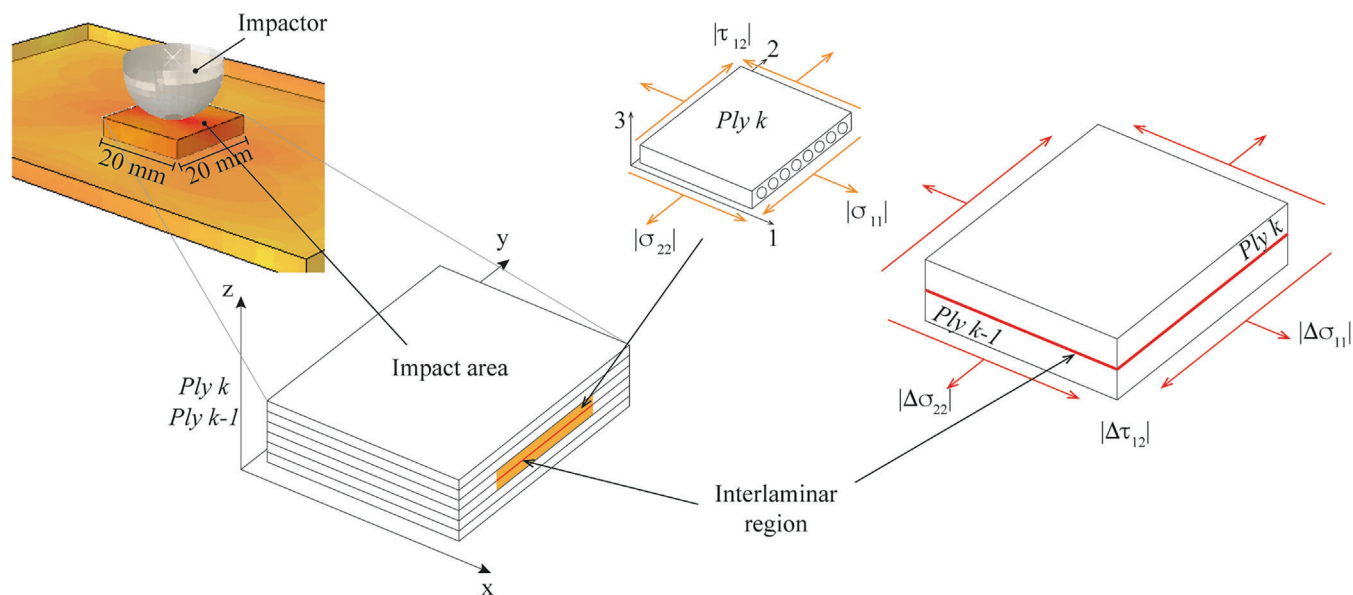
FIGURE 1 Representation of the finite elements model.

TABLE 2 Lamina's engineering constants.

E_{11}	$E_{22} = E_{33}$	$G_{12} = G_{13} = G_{23}$		
GPa	**GPa**	**GPa**	v_{12}	$v_{13} = v_{23}$
99.78 ± 9.38	6.45 ± 0.09	2.96 ± 0.05	0.32 ± 0.04	0.017 ± 0.001

results of the reference laminate under an impact of 13.5 J energy. The normal ($|\sigma_{11}|$ and $|\sigma_{22}|$) and shear ($|\tau_{12}|$) stress fields on each ply were evaluated in a 20 mm square area just under the indenter (indentation region), as illustrated in Figure 1. The mesh used in this region was composed by 0.1 mm wide square in-plane (xy) element across the thickness. Table 2 presents lamina's engineer constants used in the model and experimentally determined in.[46]

To determine the interlaminar in-plane stresses between two generic plies, we calculated the stress difference between the top integration points of the ply k-1 (bottom ply) and the corresponding stress in the bottom of the ply k (ply above). This procedure was performed for all pairs of integration points in the impact area as shown in Figure 1.

For the propose of this study, the most critical interfaces were considered those presenting largest mismatch of stresses between two generic adjacent plies (interlaminar stresses), called from now on critical interfaces in this paper.

Although minor, fibers in veils can become slightly oriented during the manufacturing process. As a result, thermal stresses may develop during the curing process, causing the laminate to physically bend and twist due

to the anisotropic in-plane coefficient of thermal stresses. To minimize this effect, a symmetric interleaving strategy was imposed. Accordingly, the FEA model identified the three most critical interlaminar regions across the laminate, and the remaining three interfaces were set symmetrically.

4 | RESULTS

4.1 | FE model

In Figure 2A–C are graphically represented the interlaminar regions with large normal (axial $|\Delta\sigma_{11}|$ and transversal $|\Delta\sigma_{22}|$) and shear ($|\Delta\tau_{12}|$) stresses, respectively. For each case, the three most critical interlaminar regions are highlighted by a red line while a green line identifies their respective symmetries. Based on the results, the highest interlaminar stresses are located near the top of the specimen on the compression side. The most critical interlaminar normal stresses, $|\Delta\sigma_{11}|$ and $|\Delta\sigma_{22}|$, share the same locations: interfaces 1, 2 and 3, while the larger interlaminate shear stresses were identified on interfaces 1, 4 and 5.

To summarize, based on the given criteria, the top six interlaminar regions for normal stresses are: 1st, 2nd,
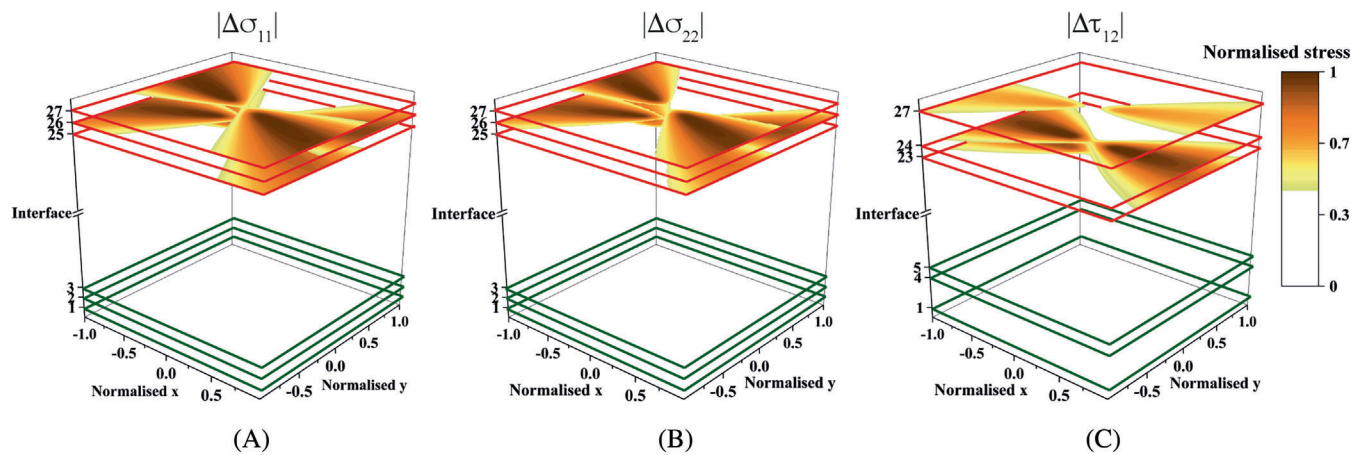
FIGURE 2 In red the three most critical (maximum) interlaminar normal, (A) $|\Delta\sigma_{11}|$ and (B) $|\Delta\sigma_{22}|$) and shear (C) $|\Delta\tau_{12}|$ stresses, respectively. In green their respective symmetric interfaces.

Veil	Glass fiber	Carbon fiber	Aramid fiber	Polyester fiber
S_f (m²/m²)	2.56	6.64	2.65	1.40
Coverage (%)	46.6 ± 2.0	70.8 ± 3.1	57.0 ± 4.2	56.0 ± 6.1

TABLE 3 Results of veils' specific surface area (S_f) and coverage (± standard deviation).
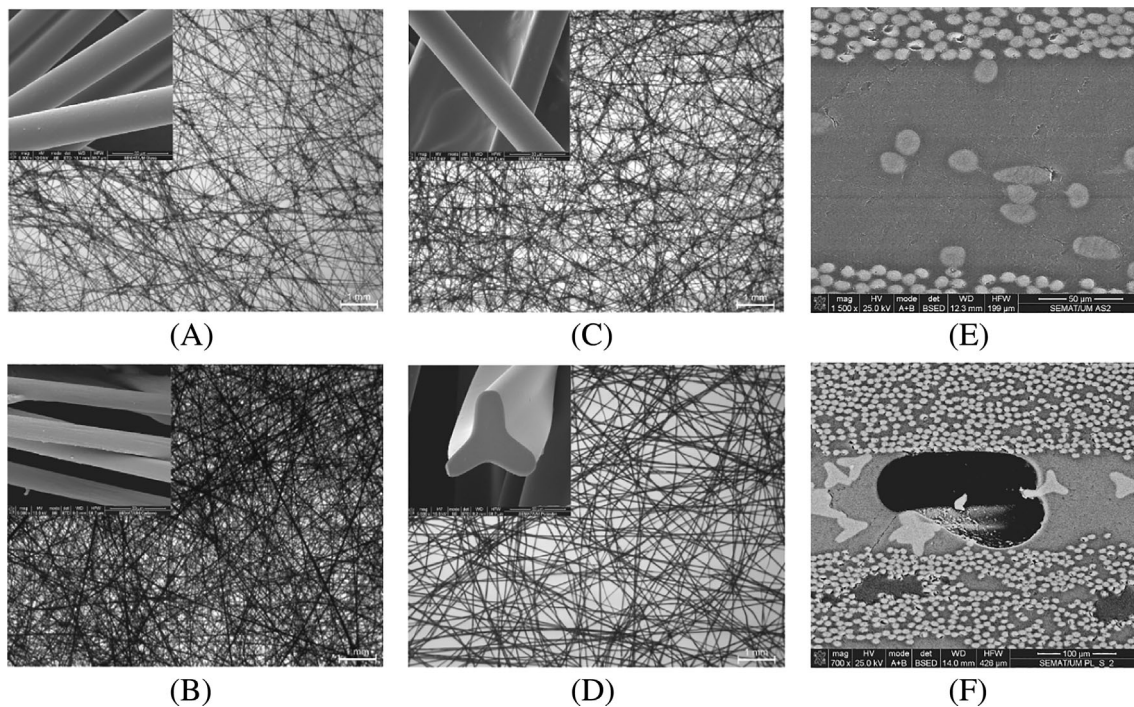
FIGURE 3 Images under transmission microscopy and, in the top left, SEM images of their fibers magnified 5000 times, where (A) is glass, (B) is carbon, (C) is aramid and (D) is polyester. Characteristic SEM images of (E) aramid veil reinforced interlaminar region and (F) a void in polyester veil interleaved laminate.

3rd, 25th, 26th, and 27th. For shear stresses, the top interfaces are: 1st, 4th, 5th, 23rd, 24th, and 27th.

The layup arrangements corresponding to both strategies are presented in Table 1.

4.2 | Raw materials characterization

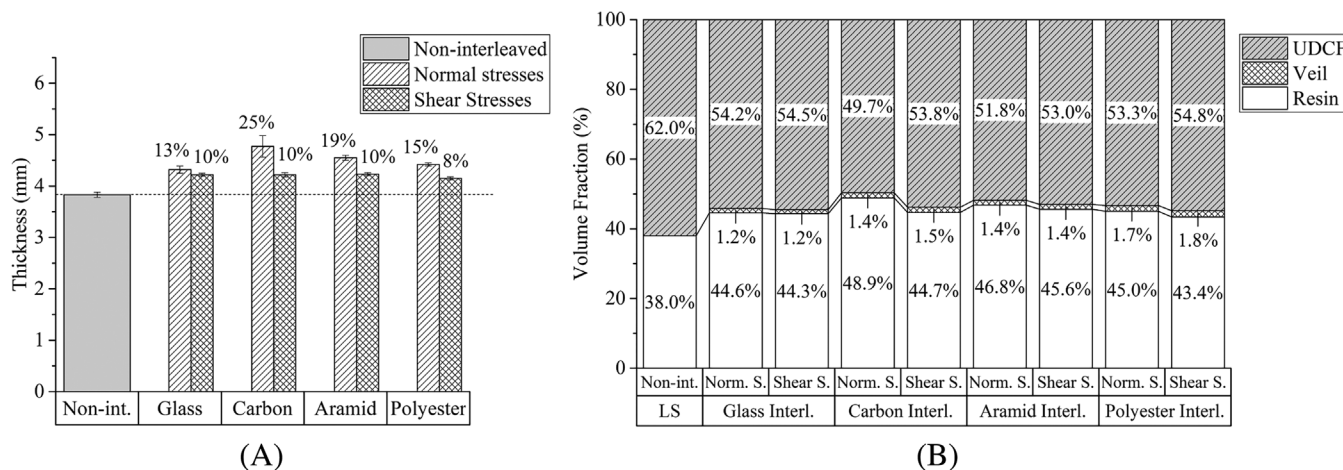Experimental results of veils' specific surface area (S_f) and coverage are presented in Table 3.

FIGURE 4 Comparison between non- and interleaved laminates (A) thickness; (B) component volume content.

Figure 3A–D presents representative black-and-white photography of glass, carbon, aramid, and polyester veils, respectively, under transmission microscopy. The coverage of each veil was experimentally determined by evaluating the percentage of dark area that covers the white background surface. As intuitively expected by comparing the four photographs, the results clearly indicate that the carbon fiber veil delivers superior coverage, followed then by aramid, polyester, and glass, respectively. Less coverage may suggest large resin-rich areas, as can be seen in Figure 3E, and an easy impregnation. On the other hand, the low resin flow on vacuum bag infusion may lead to trapped air inside low-coverage veils, as shown in Figure 3F. A deeper discussion on this subject is provided in Section 5.1.

A representative SEM image of one of its fibers is presented in the left-top corner of each veil photography. The images revealed that polyester fibers have a trilobal cross-section (Figure 3D), whereas all the others have circular cross-sections (Figure 3A–C). Images analysis also allows us to measure fibers' characteristic perimeter and determine each veil's specific surface area (S_f). Results showed that the carbon fiber veil has the highest potential contact area with the matrix, followed by aramid, glass and polyester veils.

The results indicate that the carbon fiber veil will offer higher delamination resistance since two energy dissipation mechanisms are competing: matrix/fiber debonding, provided by the high S_f, and constant front crack redirecting, from the high coverage.[37] On the other hand, the lower coverage of the glass fiber veil indicates better impregnation and fewer dry areas due to the resin flow resistance during the vacuum bag infusion process.

4.3 | Laminate characterization

The experimental measurements of laminates' thickness and volume content of their constituents are presented in Figure 4A,B, respectively. Compared to non-interleaved layup, interleaved laminates have increased by at least 8% in thickness and 5% in resin volume fraction. Furthermore, these increments had shown to be more prominent when the critical normal stresses interleaving strategy was used. This is particularly visible on carbon fiber veils interleaved laminate, which shows an increase in thickness of 25% and 11% in resin volume fraction compared to non-interleaved laminate.

In Figure 3E is presented a representative image of interleaved regions morphology observed by SEM. As may be seen, these regions are characterized by large resin-rich areas due to veils' higher porosity when compared to UDCF plies. From such observations, it was also possible to visualize a small number of voids in the laminates (Figure 3F). When the critical normal stresses strategy was adopted, few voids were mostly found in or close to the interleaved regions. In contrast, a negligible number of voids were observed dispersed into the laminate when the shear stresses strategy was applied. On the other hand, no voids were found in the reference laminate.

4.4 | Drop-weight low velocity impact results

Figure 5 shows the LVI load versus displacement curves for each layup, at the three impact energy levels of LVI. Curves overlapping at the different impact energy levels confirm tests' reliability.
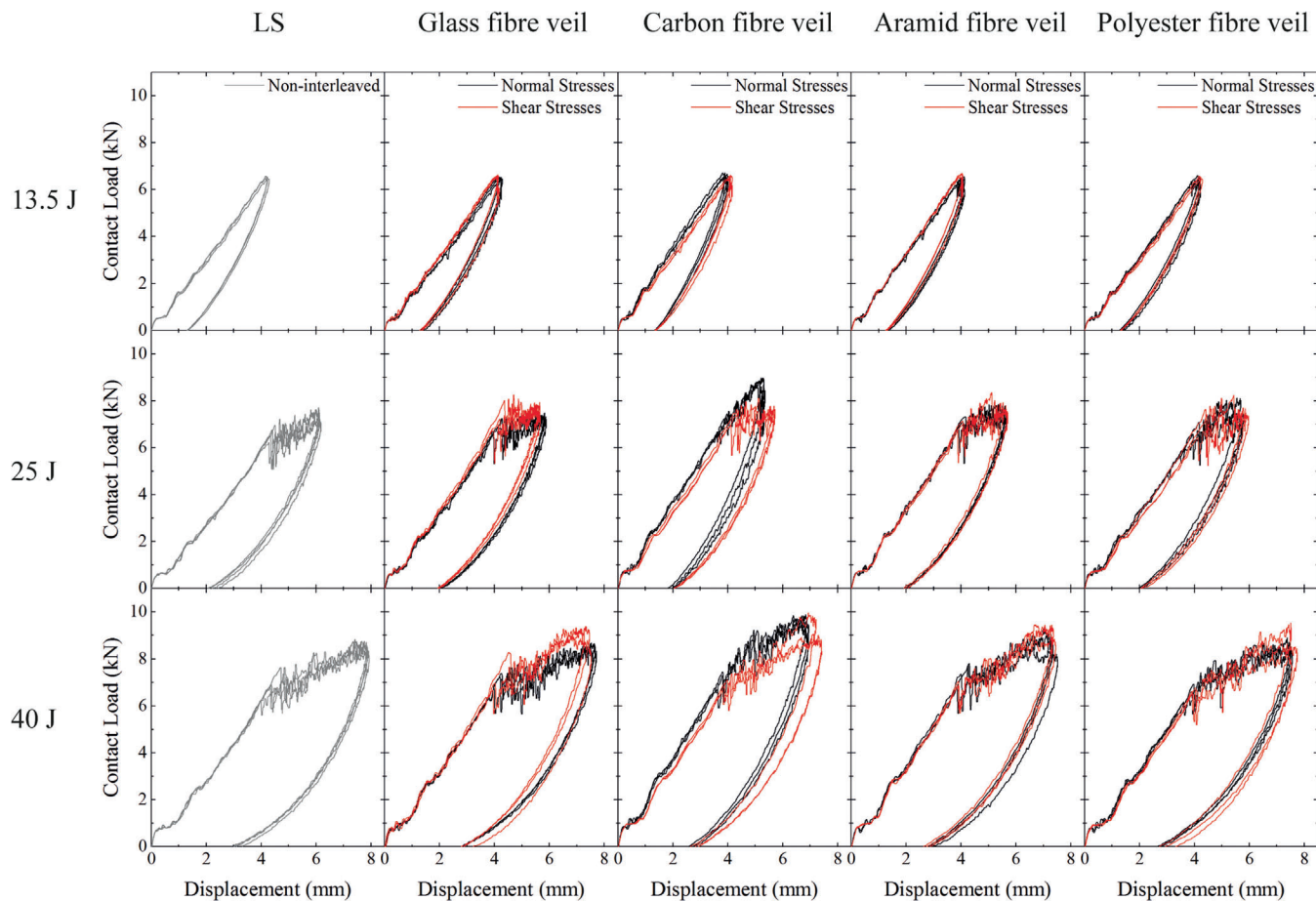
FIGURE 5   Load versus displacement curves at the three impact energy levels.

To better analyze the LVI mechanical response of each configuration, four key indicators were considered: peak load, final absorbed energy (E_{abs}), critical load (P_{cr}) and critical energy (E_{cr}). Peak load and E_{abs} show maximum load-bearing and energy absorbed during impact. On the other hand, P_{cr} and E_{cr} correspond to the load and energy registered when severe damages initiate, correspondingly. Such damage indicators can be identified in LVI load versus displacement curves by a sudden load drop, denoting a loss in stiffness and suggesting the formation of critical damages, such as delaminations or fiber breakage.[3] Thus, the maximum load recorded just before the drop indicates the load and correspondent energy needed to onset severe damages. It is also important to note that, up to this point, only sub-critical damages such as matrix cracking are formed, and most of the energy is elastically transformed.

In this work, this critical threshold was particularly visible at 25 and 40 (J) of impact energy, occurring in all tested specimens under these conditions. On the other hand, at 13.5 J, this damage indicator depends on the laminate configuration. Although all non-interleaved

specimens showed P_{cr}, no specimens of polyester veil interleaved layup on the critical shear stress interfaces exhibited this indicator. In contrast, only one specimen from all other configurations showed such a damage indicator.

The impact response of composites is greatly influenced by their thickness.[52,53] Therefore, to fairly compare the performance of laminates, all LVI mechanical indicators were normalized to their thicknesses.

Figure 6A–D show normalized results for peak load, P_{cr}, E_{abs}, and E_{cr} at three impact energy levels. After normalizing, non-interleaved laminate demonstrated slightly better mechanical performance than the new strategically interleaved configurations. Moreover, the most critical shear stress interleaving strategy typically outperformed critical normal stresses approach, regardless of the type of veil used. It is also interesting to observe that the type of veil did not seem to play a relevant role in impact mechanical response since no notorious differences were observed between laminates tested at the same impact energy, interleaved with the same strategy using different veils.
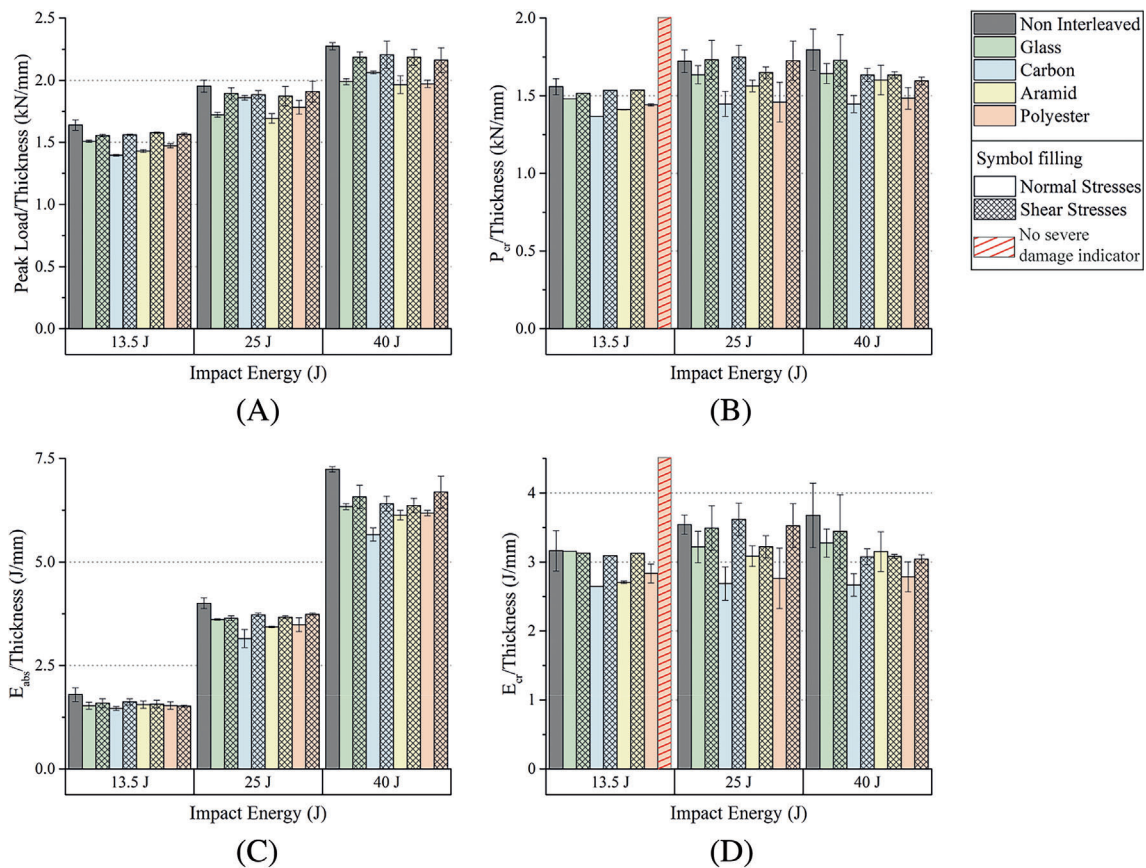
FIGURE 6 Normalized (A) peak load, (B) P_{cr}, (C) E_{abs} and (D) E_{cr} of each layup for the three impact energy levels.

4.4.1 | Visual inspections

Only a few interleaved laminates specimens showed external damage at 13.5 J, while above 25 J, all specimens showed visible back-face damages.

At 13.5 J, the interleaved laminates showed no significant differences in their back-face failure mode. All laminates developed small fiber breakage on their back faces under the impactor, except for the laminate interleaved with polyester veils using the shear stresses strategy, which remained undamaged. Non-interleaved laminate specimens developed localized matrix splitting. At 25 J, all laminates exhibited fiber breakage on their back-face, surrounded by small and localized matrix splitting.

At 40 J, most of the interleaved layups experienced a combination of fiber breakage and extensive matrix splitting. The only exception was the laminate interleaved with carbon veils at the most critical shear stress interfaces, which exhibited extensive matrix splitting similar to what was observed in the non-interleaved configuration.

Figure 7 shows photographs of characteristic back-face failure mode developed on each laminate at 40 J of impact energy.

Figure 8 shows the extent of back-face damage, λ, measured in each laminate. As observed in other studies,[3] as the impact energy level increases, the damage on the back face of the specimens becomes more extensive. Furthermore, regardless of the veil used, all laminates where the critical shear stress strategy was adopted have developed smaller damages than the non-interleaved layup, contrary to those interleaved on critical normal stress interfaces.

4.4.2 | Internal damage area after impact

Ultrasonic C-scan inspections were carried out both before and after the impact tests. The inspections conducted before the impact tests showed a consistent ultrasound signal, which allowed the failures in the signal observed during the C-scan inspection of impacted specimens to be identified as damage caused by LVI tests.

An ultrasound C-scan was used to evaluate the area and shape of internal damage. It was found that when the impact energy was at 13.5 J, all laminates formed circular internal damages. However, at higher energies, such as 40 J, the damages became oval-shaped, as shown in the grayscale C-scan images in Figure 9.
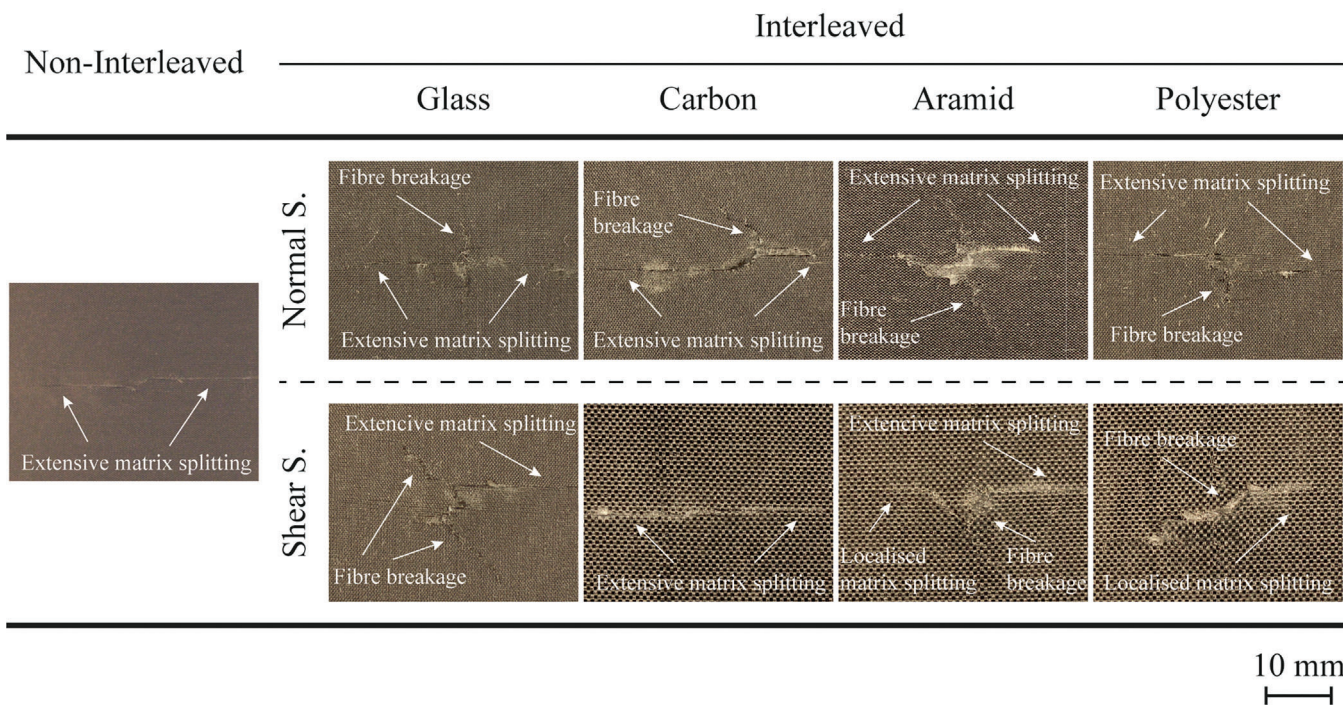
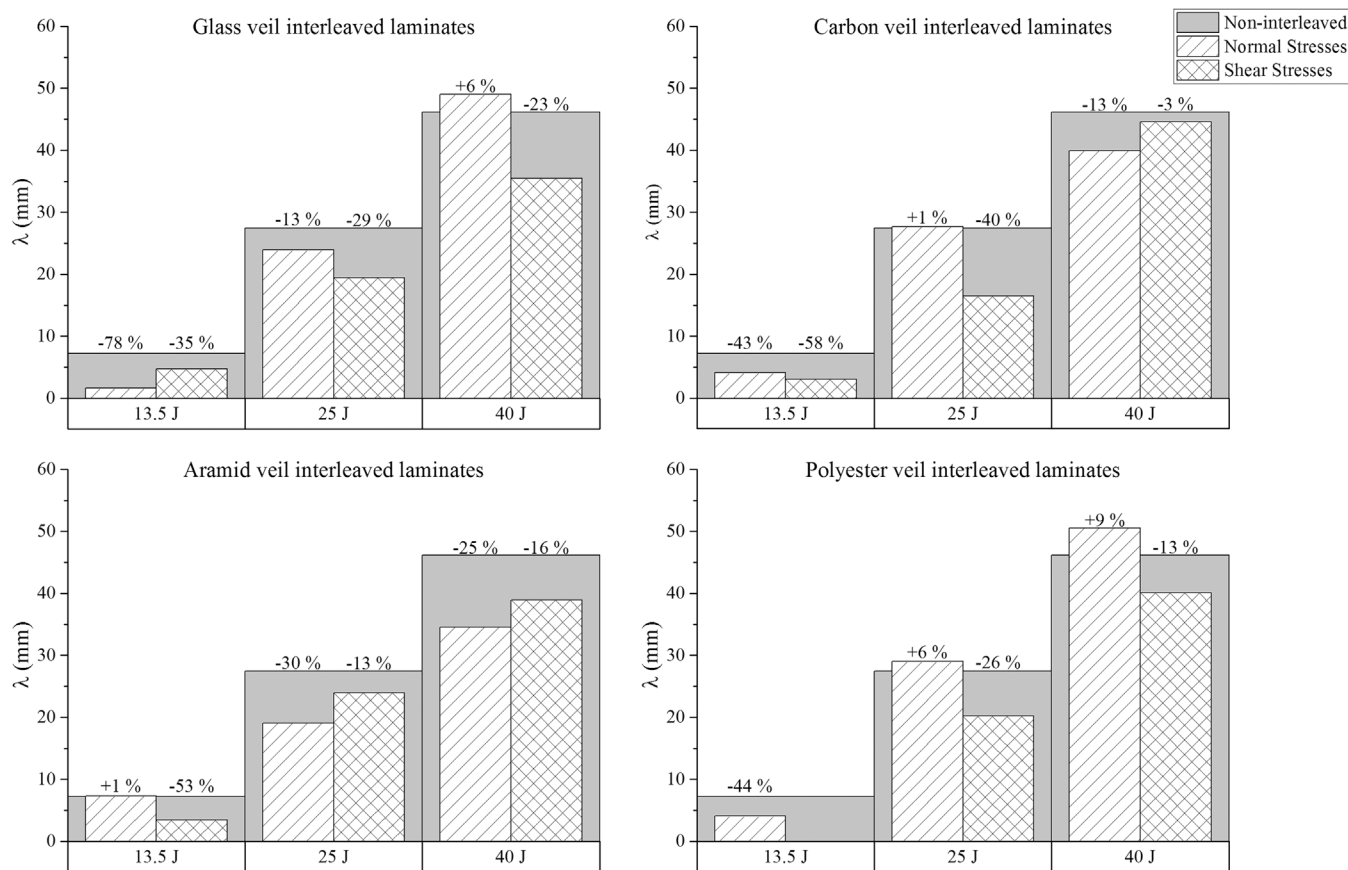**FIGURE 7**   Characteristic back-face failure mode developed at 40 J.

FIGURE 8   Back-face damage extent (λ) on each interleaved laminate and its variation to non-interleaved at each impact level.
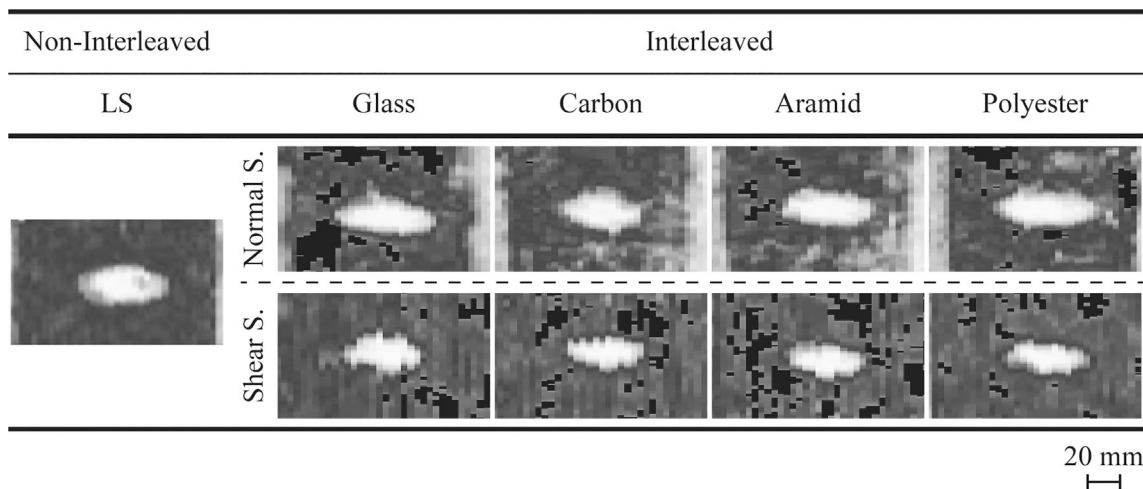
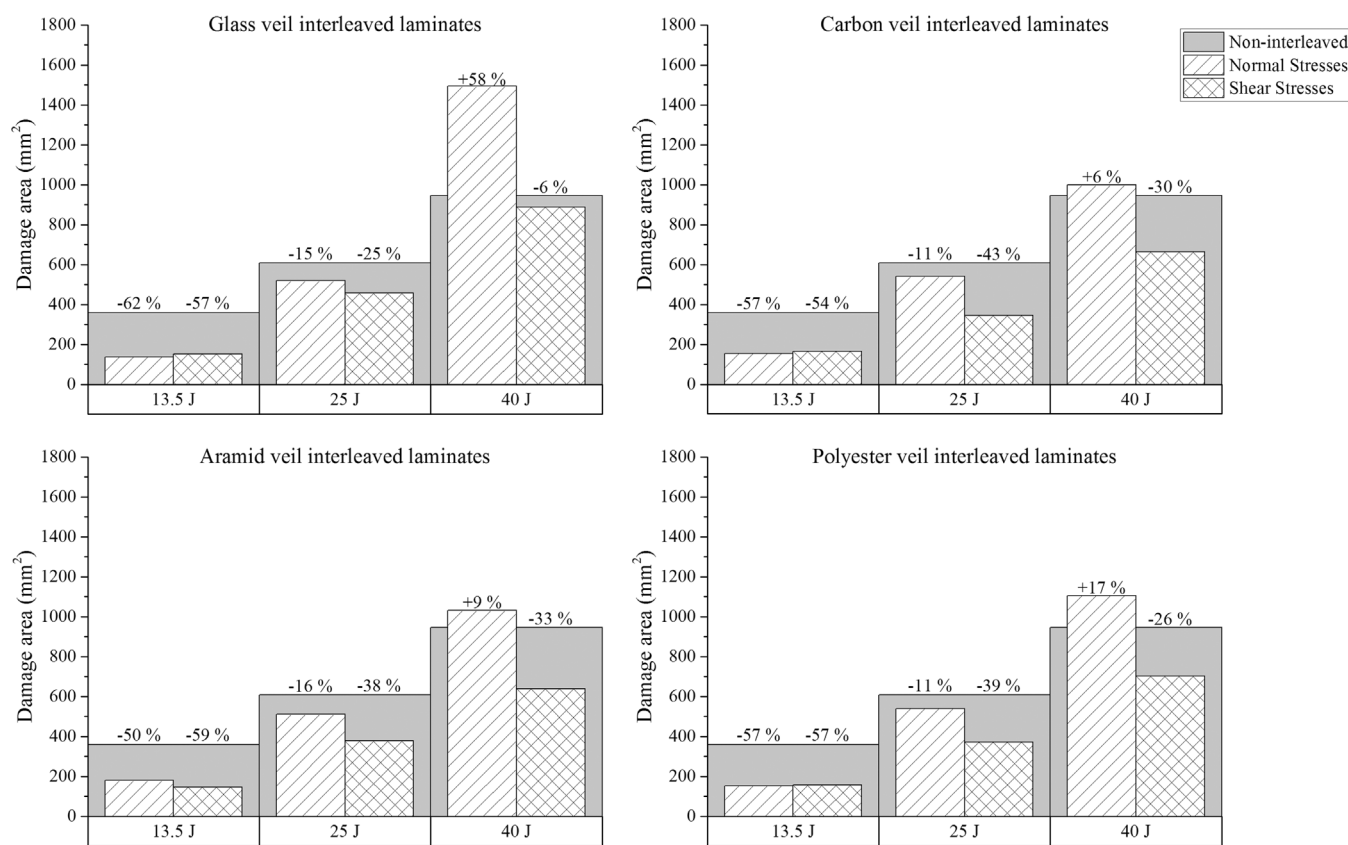**FIGURE 9** Grayscale C-scan images of each laminate impacted at 40 J.

FIGURE 10 Internal damage area of each interleaved layup and its variation to non-interleaved at each impact level.

Figure 10 presents the internal damage areas measured in all specimens. It can be observed that regardless of the interleaving strategy or veil type, all laminates that were interleaved developed smaller damages than the non-interleaved configuration when subjected to 13.5 and 25 J impact energy. However, at 40 J impact energy, laminates interleaved at critical normal stress interfaces developed more significant damages than the non-interleaved ones. It is important to note that the critical shear stress strategy outperforms both the non-interleaved and interleaved laminates on the most critical normal stress interfaces. At 25 and 40 J of impact energy, this approach significantly reduces the internal damage area.

5 | DISCUSSION

5.1 | Laminates' characterization

The resin-rich areas observed in Figure 3E mainly result from the high permeability of veils compared to UDCF layers, leading to an overall increment of laminates' volume. This resulted in a higher resin volume fraction of interleaved laminates and up to 25% increment in thickness compared to the non-interleaved configuration, as seen in Figure 4A. The thickness of such interlaminar regions may play a role in mechanical performance and impact damage resistance depending on their location in the layup, as will be discussed later. Thicker interleaved regions lead to higher resin volume fraction in the interlaminar region, decreasing stiffness and toughness, which typically leads to larger delamination areas.[41,42]

Laminates interleaved with shear stress had less thickness increase than those with critical normal stress. This indicates different impregnation and veil relaxation during the vacuum bag infusion process. Further study is needed to understand this phenomenon. Nevertheless, the superior thickness observed on interleaved laminates, generically, led to superior LVI mechanical indicators, as peak (bending) load as well as damage onsetting load and energy on these configurations. However, as mentioned above, to minimize the effects of geometry, all mechanical properties obtained were normalized to the thickness of their respective configuration in this work.

The observation of the laminates' cross-section revealed a few voids inside most interleaved configurations (Figure 3F), in contrast, no voids were found in the non-interleaved layup. Typically, they were found within interleaved layers and mostly on interleaved laminates where the critical normal stress strategy was adopted. Based on literature,[54] voids formation in vacuum bag infusion process is primarily attributed to the resin flow and porosity of the fibrous medium. This process has a relatively slow resin flow, which means capillary flows are dominant over hydrodynamic ones. As a result, UDCF are impregnated first due to the small gaps between fibers and their higher superficial tension. This can lead to air entrapments in more porous mediums such as veils. Therefore, their apparently higher compaction and lower thickness justify the smaller number of voids found in shear stresses interleaved laminates.

5.2 | Mechanical behavior under low velocity impact (LVI) tests

Figure 6 shows that most interleaved laminates have inferior mechanical indicators to non-interleaved ones under LVI tests. However, in most cases, critical shear stress strategy performs better than critical normal stress', regardless the interleaved veil. This overperformance is clearly visible for the peak load and E_{abs} in Figure 6A,C, respectively. On the contrary, critical normal stress strategy apparently depend on the veil type, however, no trend is identified for different impact energy levels. As an example, carbon fiber veil shows interleaved composites lower load-bearing capability and absorbed energy at 13.5 J. Although they present the highest peak load at 40 J, while absorbed energy remains the lowest among.

Regarding the severe damage indicator, results at 13.5 J revealed that critical shear stress strategy presented similar P_{cr} and E_{cr} values as the reference (Figure 6B,D), except polyester veil interleaved laminate, where no damage indicators were found. Conversely, the critical normal stress strategy was found to be more susceptible to severe damages at lower impact energy levels. At 25 J, critical shear stress strategy using glass, carbon and polyester veils had similar values of P_{cr} and E_{cr} than the reference. However, in all other configurations where the normal stress strategy was adopted, those values were lower, suggesting higher susceptibility of these laminates to develop severe damages under intermediate loading conditions. At 40 J, regardless of the interleaving strategy used, all interleaved laminates presented slightly lower damage indicators compared to reference. It is important to note that, once again, the shear stress interleaving strategy proved to be more effective than the normal stress approach in most cases.

To summarize, critical shear stress interleaved laminates outperformed those where the normal stress strategy was used regarding load and energy needed to trigger the first severe damage, P_{cr} and E_{cr}, respectively. However, no correlation was possible to establish regarding the type of veil used. Furthermore, the overall superior mechanical performance of critical shear stress interleaved configurations indicates that interleaving strategy plays a more significant role than the type of veils selected. The higher number of stiffer layers of UDCF close to the outer surfaces compared to the normal stresses interleaving approach, provides higher bending resistance, generically addressing better mechanical performances to these laminates.

Nevertheless, the higher number of voids observed on configurations where the normal shear stress strategy was applied, compared to all the other layups, may have a negative influence on their mechanical performance. To clarify this hypothesis, additional studies need to be conducted.

5.3 | Low velocity impact (LVI) damage resistance

5.3.1 | Role of interleaving strategy on impact damage

Figure 8 compares the back-face damage extent (λ) among the different laminates after impact. The labels above the patterned bars indicate the deviation of interleaved laminates from the non-interleaved reference.

As may be seen, regardless of the impact energy level, laminates strategically interleaved on critical shear stress interfaces always exhibited less back-face damage compared with the non-interleaved layup, while more extensive damages were observed in some cases where the critical normal stress strategy was employed. At 13.5 J, the best performance was achieved by the laminate interleaved with the polyester veil on the critical shear stress interfaces, where no damage was observed in any specimen. On the other hand, configuration with the aramid veil on critical normal stress revealed the worst performance with a similar damage extent to the reference. All the other interleaved configurations showed a significant reduction in external damage. In particular, laminate interleaved with glass on the critical normal stress showed impressive performance, reducing its external damage by 78%, compared to the reference.

At 25 J, most interleaved structures showed to be less prone to develop extensive damages compared to the reference, with the only exception being the layup interleaved with an aramid veil on most critical normal stress interfaces. It should be noted that laminates interleaved with carbon and polyester veils demonstrated antagonistic performances simply by changing the interleaving strategy. In both cases, when the critical shear stress strategy was applied, a damage reduction of about 40% and 26% was observed in laminates interleaved with carbon and polyester veils, respectively. On the other hand, when these veils were placed on the most critical normal stress interfaces, both laminates presented slightly larger damages compared to the reference.

Regardless of the interleaving approach, at 40 J, laminates interleaved with carbon and aramid veils formed smaller damages compared to the reference. The better performance was achieved by the laminate interleaved with the aramid veil on the critical normal stress interfaces, with a reduction of 25% compared to the reference. On the other hand, depending on the strategy, laminates interleaved with glass and polyester veils revealed opposite behavior. When placed on critical shear stress interfaces, they developed smaller damages than the reference, by 23% and 13%, respectively. On the contrary, when the critical normal stress interleaving strategy was implemented, both layups revealed more significant damages than the same reference.

It is well known that under LVI, composite laminates can develop internal damages almost imperceptible to the naked eye, the so-called Barely Visible Impact Damage (BVID). Figure 10 compares internal damage areas developed on interleaved and non-interleaved laminates at each impact energy level. Irrespective of the interleaving strategy, up to 25 J impact energy, interleaved laminates developed smaller internal damages than the reference. Furthermore, regardless of the impact energy, laminates interleaved at critical shear stress interfaces continuously developed fewer damages than the reference. This interleaving strategy also demonstrated to be less sensitive to damage formation, especially at higher energy levels (25 and 40 J), showing a damage area variation between −6% and −43%, whereas the normal stress interleaving strategy presented a variation from −16% to +58% compared to the reference. At 13.5 J, all interleaved laminates demonstrated an impressive damage resistance compared to the reference, reducing damage area by 62%–50%. At 25 J, all interleaved layups also outperformed the non-interleaved. However, the critical normal stress strategy reduced damage area by 16%–11%, whereas the shear stress interleaving strategy exhibited reductions of up to 43% (carbon veil interleaved laminates). The superior performance of laminates interleaved at critical shear stress interfaces was further confirmed at an impact energy of 40 J, where they developed fewer damages than all the other laminates. Moreover, while the shear stress interleaving strategy decreased the impact damage area by up to 33% (aramid veils), all laminates interleaved at critical normal stress interfaces developed damages at least 6% larger (carbon veil) than the reference.

In summary, the LVI damage resistance analyses presented here revealed the importance of the interleaving strategy on damage formation and propagation in composite laminates. As observed, the critical shear stress interleaving strategy consistently outperformed all other configurations in terms of both external and internal damage, regardless of the interleaved veil or impact energy. On the other hand, the role of the nature of the interleaved veil showed an erratic performance, depending on the interleaving strategy approach and impact energy. These results suggest that the interleaving strategy is crucial in mitigating LVI damage formation in laminate composites. In particular, incorporating veils into interlaminar regions with higher in-plane shear stress gradients between adjacent plies significantly improves composite laminates' resistance to LVI impact damage. Nevertheless, must be noted that depending on the application or service environment conarium, the selection of veils may be an essential rule in the materials selection
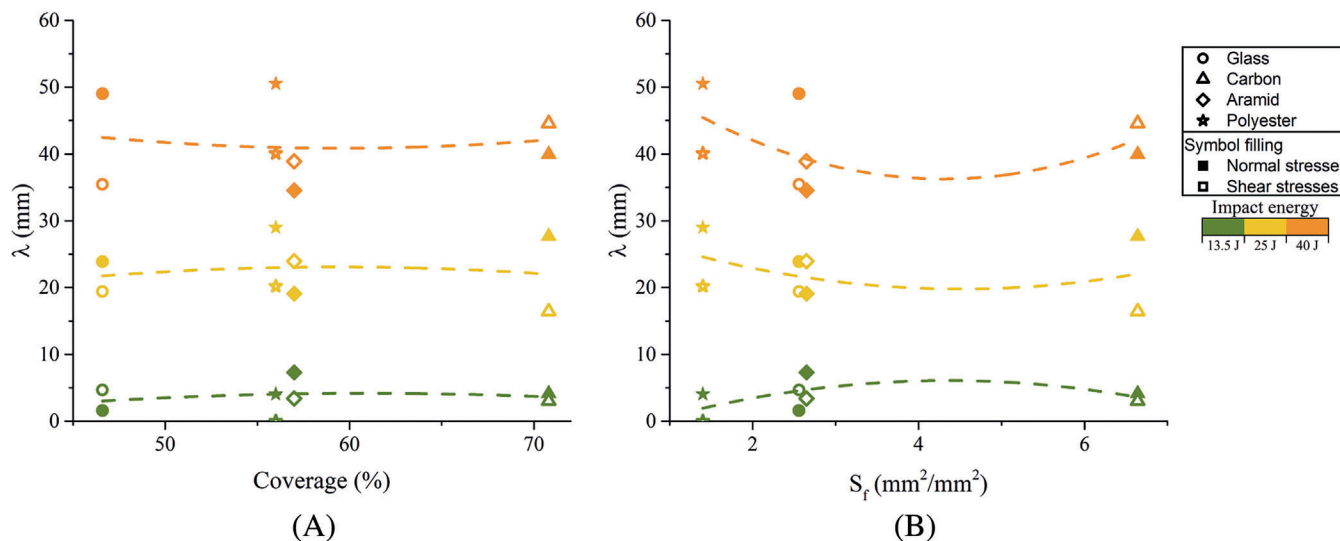
FIGURE 11 Back-face damage extent (λ) versus (A) covered surface area and (B) specific surface area on interleaved laminates.

stage. Properties such as areal density, moisture and water absorption ratio, or the coefficient of thermal expansion may introduce additional weight or dimensional uncertainty in service, which can increase operational costs and accuracy concerns in some industries, such as aerospace.

5.3.2 | Role of veils microstructural network on impact damage

The role of veils' microstructure, namely coverage and the specific surface area, is considered in this section to evaluate their effect on back-face and internal damage.

Figure 11A,B show the evolution of back-face damage extent (λ) against veils' coverage and specific surface area, S_f, respectively, of interleaved laminates at the three impact energy levels. From the trendlines plotted in Figure 11A for each impact energy level, it may be concluded that veils' coverage did not have any influence on back-face damage extent, contrary to S_f, which seems to play a much more important role (Figure 11B).

At 13.5 J, laminates interleaved with intermedium S_f veils (glass and aramid veils) developed slightly more extensive back-face damage than those with smaller and larger S_f, polyester and carbon veils, respectively. Nevertheless, not all specimens presented external damages at this impact energy level, suggesting that 13.5 J is the impact energy threshold for developing back-face damage under these conditions. Therefore, no correlation can be made between different laminate configurations. At 25 and 40 J, yellow and orange trendlines, laminates interleaved with the lowest S_f, specifically the polyester veil, contributed slightly to larger external damages.

Referring to Figure 12A, for internal damage and up to 25 J of impact energy, veils' coverage did not significantly influence its formation. Nevertheless, a stronger correlation was observed at the highest impact energy level. At 40 J, laminates interleaved with a glass fiber veil (lowest coverage) developed larger damages. While this veil's characteristic increased, smaller damages were progressively observed.

Figure 12B displays the internal damage area plotted against the veils' specific surface area. As observed, up to 25 J, internal damage seems independent of S_f. However, at 40 J, laminates interleaved with intermediate S_f (glass and aramid) developed more extensive damage than those with lower and larger S_f.

Accordingly, external back-face damage seems more dependent on veil S_f than on coverage, suggesting that fiber bridging, rather than matrix cracking, is the primary damage mechanism forming this type of damage. On the other hand, internal damage primarily depended on the interleaving strategy used, while the microstructure of the veils only seems to play a role in higher impact energies. In these conditions, laminates interleaved with veils of low coverage developed larger damages, indicating that cracks grow preferentially through the resin-rich medium. Contrarily, when gaps between veils' fibers are smaller, cracks tend to be constantly redirected, dissipating more energy and leading to minor damages. Similarly, laminates interleaved with veils of high S_f, such as the carbon veil, also have higher impact damage resistance. This may result from more energy expended on debonding and fiber bridging.

Interestingly, laminates interleaved with the polyester veil, which has the lowest S_f, revealed a performance comparable to the carbon veil interleaved layup.
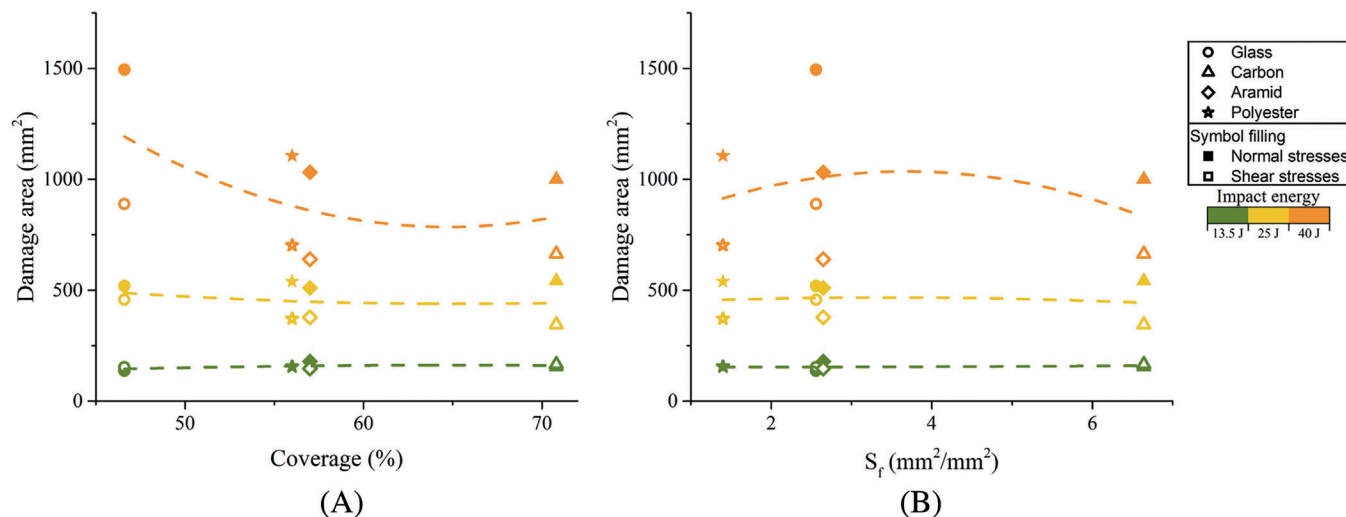
FIGURE 12 Influence on interleaved laminates internal damage area of (A) covered surface area and (B) specific surface area.

The justification of such results may rely on the trilobal geometry of polyester fibers. According to M. Herráez et al.,[55] trilobal cross-section fibers tend to develop higher residual interfacial stresses, comparatively to circular cross-section fibers, which results in easier interfacial debonding. On the other hand, J. Mohan et al.[56] studied the interlaminar fracture toughness, in mode I, of composite joins using epoxy film reinforced with trilobal cross-section polyester fibers. Under microscope, they observed some cracks growing against the main crack direction. Based on those observations, it's plausible that both phenomena contribute to higher energy dissipation and, consequently, improved damage resistance. Despite out of the main focus of this work, the slight trends and observations presented here regarding the role of veils' microstructural network in LVI damage formation deserve careful consideration in future research. Of particular interest is the influence of the fibers cross-section geometry of interleaving veils on impact energy dissipation, as this is a subject that has been poorly studied to date.

6 | CONCLUSIONS

The influence of the interleaving strategy on low velocity impact damage resistance of composite laminates was investigated in this work. A conventional baseline aircraft laminate was modified at the interlaminar regions with the most significant in-plane interlaminar stress, as previously identified in an FEA simplified quasi-static model. Accordingly, two interleaving location sets were defined: the most considerable in-plane normal (axial/transverse) stress and in-plane shear stress mismatch between adjacent laminae. Four veils, made of glass, carbon, aramid and polyester fibers, were used as interlaminar toughening systems to validate the proposed strategic interleaving approach. Interleaved and non-interleaved laminates were produced by vacuum bag infusion under the same conditions.

Laminates' characterization showed an increase in thickness and resin volume fraction, both interleaving strategies. It was especially visible when the critical normal stress strategy was applied, reaching 25% and 11%, respectively, compared to the non-interleaved laminate. SEM observations revealed interleaved resin-rich regions punctuated with few voids in contrast with the reference. Non-interleaved laminate revealed higher LVI mechanical indicators, namely, peak load, P_{cr}, E_{cr} and E_{abs}, than the most interleaved layups. Among the interleaved configurations, shear stress strategy interleaved layups, generically, have demonstrated superior mechanical performance. It terms of LVI damage resistance, both interleaving strategies led to an improvement, reducing, in most cases, internal and external impact damage compared to the reference laminate. Regardless of impact energy, interleaving shear stresses showed remarkable results in preventing external damage and reducing internal damage up to 59% at 13.5 J. At 25 J, it mitigated external and internal damage by 40% (carbon veil), and at 40 J, those damages were reduced by 33% (aramid veil) and 23% (glass veil), respectively. Nevertheless, no correlation was observed between the type of veil (material) used and the impact damages. This indicates that the interleaving strategy is more vital in LVI damage resistance than the veils' material. Results also revealed that veils with intermediate specific surface area, Sf, seem to reduce back-face damages, while high coverage veils can

significantly constrain delaminations at higher impact energies (40 J). From the results, it is clear that a thorough analysis of interlaminar stresses in a laminate and implementing an appropriate interleaving strategy can effectively reduce LVI damages. Despite the promising results, further work must be carried out to understand better the relationship between veils' network structure and LVI damage resistance, as well as the veil's location in the laminates and voids formation during the vacuum bag infusion process. It would also be interesting to evaluate the performance of the newly proposed interleaving approach using pre-impregnated material systems and different composite manufacturing processes, such as resin transfer molding (RTM) or autoclave. This interleaving methodology significantly enhances the LVI damage resistance of composites in high-demanding applications, leading to reduced thickness, increased fiber volume fraction, and decreased maintenance costs.

DATA AVAILABILITY STATEMENT

The data that support the findings of this study are available from the corresponding author upon reasonable request.

ORCID

L. Amorim https://orcid.org/0000-0002-8583-3380

REFERENCES

1. Administration FA. Aviation maintenance technician handbook - airframe. *Aviat Maint Tech Handb - Airframe*. 2012;1:588. doi:10.1017/CBO9781107415324.004
2. Gardiner G. Aerocomposites: The move to multifunctionality: CompositesWorld. http://www.compositesworld.com/articles/aerocomposites-the-move-to-multifunctionality. Published 2015. Accessed July 14, 2017
3. Cheng Z, Xiong J. Progressive damage behaviors of woven composite laminates subjected to LVI, TAI and CAI. *Chin J Aeronaut*. 2020;33(10):2807-2823. doi:10.1016/j.cja.2019.12.015
4. Gnädinger F, Middendorf P, Fox B. Interfacial shear strength studies of experimental carbon fibres, novel thermosetting polyurethane and epoxy matrices and bespoke sizing agents. *Compos Sci Technol*. 2016;133:104-110. doi:10.1016/j.compscitech.2016.07.029
5. Balasubramanian M. *Composite Materials and Processing*. Vol 1. First ed. CRC Press; 2013.
6. Kaw AK. *Mechanics of Composite Materials*. Vol 29. 2nd ed. Taylor & Francis, Inc.; 2006. doi:10.1016/j.fsigen.2011.07.001
7. Jones RM. *Mechanics of Composite Materials*. 2nd ed. Taylor and Francis, Inc.; 1999. doi:10.1007/BF00611782
8. Andrew JJ, Srinivasan SM, Arockiarajan A, Dhakal HN. Parameters influencing the impact response of fiber-reinforced polymer matrix composite materials: a critical review. *Compos Struct*. 2019;224(May):111007. doi:10.1016/j.compstruct.2019.111007
9. Mouritz AP. Review of z-pinned composite laminates. *Compos Part A Appl Sci Manuf*. 2007;38(12):2383-2397. doi:10.1016/j.compositesa.2007.08.016
10. Gnaba I, Legrand X, Wang P, Soulat D. Through-the-thickness reinforcement for composite structures: a review. *J Ind Text*. 2019;49(1):71-96. doi:10.1177/1528083718772299
11. Song C, Fan W, Liu T, Wang S, Song W, Gao X. A review on three-dimensional stitched composites and their research perspectives. *Compos Part A Appl Sci Manuf*. 2022;153(October 2021):106730. doi:10.1016/j.compositesa.2021.106730
12. DeCarli M, Kozielski K, Tian W, Varley R. Toughening of a carbon fibre reinforced epoxy anhydride composite using an epoxy terminated hyperbranched modifier. *Compos Sci Technol*. 2005;65(14):2156-2166. doi:10.1016/j.compscitech.2005.05.003
13. Thomas R, Yumei D, Yuelong H, et al. Miscibility, morphology, thermal, and mechanical properties of a DGEBA based epoxy resin toughened with a liquid rubber. *Polymer (Guildf)*. 2008;49(1):278-294. doi:10.1016/j.polymer.2007.11.030
14. Ravindran AR, Ladani RB, Kinloch AJ, Wang CH, Mouritz AP. Improving the delamination resistance and impact damage tolerance of carbon fibre-epoxy composites using multi-scale fibre toughening. *Compos Part A Appl Sci Manuf*. 2021;150(August):106624. doi:10.1016/j.compositesa.2021.106624
15. Sager RJ, Klein PJ, Lagoudas DC, et al. Effect of carbon nanotubes on the interfacial shear strength of T650 carbon fiber in an epoxy matrix. *Compos Sci Technol*. 2009;69(7–8):898-904. doi:10.1016/j.compscitech.2008.12.021
16. Kepple KL, Sanborn GP, Lacasse PA, Gruenberg KM, Ready WJ. Improved fracture toughness of carbon fiber composite functionalized with multi walled carbon nanotubes. *Carbon N Y*. 2008;46(15):2026-2033. doi:10.1016/j.carbon.2008.08.010
17. Guzman de Villoria R, Hallander P, Ydrefors L, Nordin P, Wardle BL. In-plane strength enhancement of laminated composites via aligned carbon nanotube interlaminar reinforcement. *Compos Sci Technol*. 2016;133:33-39. doi:10.1016/j.compscitech.2016.07.006
18. Vallack N, Sampson WW. Materials systems for interleave toughening in polymer composites. *J Mater Sci*. 2022;57(11):6129-6156. doi:10.1007/s10853-022-06988-1
19. García-rodríguez SM, Costa J, Singery V, Boada I, Mayugo JA. The effect interleaving has on thin-ply non-crimp fabric laminate impact response : X-ray tomography investigation. *Compos Part A J*. 2018;107(January):409-420. doi:10.1016/j.compositesa.2018.01.023
20. Nash NH, Young TM, Stanley WF. An investigation of the damage tolerance of carbon / Benzoxazine composites with a thermoplastic toughening interlayer. *Compos Struct*. 2016;147:25-32. doi:10.1016/j.compstruct.2016.03.015

21. Chen L, Wu LW, Jiang Q, et al. Improving interlaminar fracture toughness and impact performance of carbon fiber/epoxy laminated composite by using thermoplastic fibers. *Molecules*. 2019;24(18):3367. doi:10.3390/molecules24183367

22. Zhang C, Zheng X, Zhu K, Peng J, Wang Z, Lan L. Experimental investigation of low-velocity impact behavior and CAI on composite laminates by discrete interleaved toughening. *Mech Adv Mater Struct*. 2022;13:1-12. doi:10.1080/15376494.2022.2158504

23. Singh S, Partridge IK. Mixed-mode fracture in an interleaved carbon-fibre/epoxy composite. *Compos Sci Technol*. 1995;55(4):319-327. doi:10.1016/0266-3538(95)00062-3

24. Chen SF, Jang BZ. Fracture behaviour of interleaved fiber-resin. *Composites*. 1991;41:77-97.

25. Cheng C, Zhang C, Zhou J, et al. Improving the interlaminar toughness of the carbon fiber/epoxy composites via interleaved with polyethersulfone porous films. *Compos Sci Technol*. 2019;183:183. doi:10.1016/j.compscitech.2019.107827

26. Rodríguez-González JA, Rubio-González C. Influence of sprayed multi-walled carbon nanotubes on mode I and mode II interlaminar fracture toughness of carbon fiber/epoxy composites. *Adv Compos Mater*. 2019;28(sup1):19-36. doi:10.1080/09243046.2018.1458510

27. Song Y, Zheng N, Dong X, Gao J. Flexible Carboxylated CNT/PA66 Nanofibrous mat interleaved carbon fiber/epoxy laminates with improved Interlaminar fracture toughness and flexural properties. *Ind Eng Chem Res*. 2020;59(3):1151-1158. doi:10.1021/acs.iecr.9b05854

28. Verma L, Jefferson Andrew J, Sivakumar SM, Balaganesan G, Vedantam S, Dhakal HN. Compression after high-velocity impact behavior of pseudo-elastic shape memory alloy embedded glass/epoxy composite laminates. *Compos Struct*. 2021;259(October 2020):113519. doi:10.1016/j.compstruct.2020.113519

29. Verma L, Sivakumar SM, Andrew JJ, Balaganesan G, Arockirajan A, Vedantam S. Compression after ballistic impact response of pseudoelastic shape memory alloy embedded hybrid unsymmetrical patch repaired glass-fiber reinforced polymer composites. *J Compos Mater*. 2019;53(28–30):4225-4247. doi:10.1177/0021998319856426

30. Lyashenko-Miller T, Fitoussi J, Marom G. The loading rate effect on mode II fracture toughness of composites interleaved with CNT. *Nanocomposites*. 2016;2(1):1-7. doi:10.1080/20550324.2016.1159372

31. García-Rodríguez SM, Costa J, Rankin KE, Boardman RP, Singery V, Mayugo JA. Interleaving light veils to minimise the trade-off between mode-I interlaminar fracture toughness and in-plane properties. *Compos Part A Appl Sci Manuf*. 2020;128(October 2019):105659. doi:10.1016/j.compositesa.2019.105659

32. Quan D, Alderliesten R, Dransfeld C, Murphy N, Ivanković A, Benedictus R. Enhancing the fracture toughness of carbon fibre/epoxy composites by interleaving hybrid meltable/non-meltable thermoplastic veils. *Compos Struct*. 2020;252(June):112699. doi:10.1016/j.compstruct.2020.112699

33. Quan D, Mischo C, Binsfeld L, Ivankovic A, Murphy N. Fracture behaviour of carbon fibre/epoxy composites interleaved by MWCNT- and graphene nanoplatelet-doped thermoplastic veils. *Compos Struct*. 2020;235(December 2019):111767. doi:10.1016/j.compstruct.2019.111767

34. Zhang H, Liu Y, Kuwata M, Bilotti E, Peijs T. Improved fracture toughness and integrated damage sensing capability by spray coated CNTs on carbon fibre prepreg. *Compos Part A Appl Sci Manuf*. 2015;70:102-110. doi:10.1016/j.compositesa.2014.11.029

35. Walker L, Sohn MS, Hu XZ. Improving impact resistance of carbon-fibre composites through interlaminar reinforcement. *Compos - Part A Appl Sci Manuf*. 2002;33(6):893-902. doi:10.1016/S1359-835X(02)00010-6

36. Hogg PJ. Toughening of thermosetting composites with thermoplastic fibres. *Mater Sci Eng A*. 2005;412:97-103. doi:10.1016/j.msea.2005.08.028

37. Beylergil B, Tanoglu M, Aktas E. Effect of polyamide-6,6 (PA 66) nonwoven veils on the mechanical performance of carbon fiber/epoxy composites. *Compos Struct*. 2018;194-(February):21-35. doi:10.1016/j.compstruct.2018.03.097

38. Saghafi H, Ghaffarian SR, Yademellat H, Heidary H. Finding the best sequence in flexible and stiff composite laminates interleaved by nanofibers. *J Compos Mater*. 2019;53(28–30):4065-4076. doi:10.1177/0021998319850874

39. Ramji A, Xu Y, Yasaee M, Grasso M, Webb P. Influence of veil interleave distribution on the delamination resistance of cross-ply CFRP laminates under low velocity impact. *Int J Impact Eng*. 2021;157(April):103997. doi:10.1016/j.ijimpeng.2021.103997

40. Jefferson AJ, Srinivasan SM, Arockiarajan A. Effect of multiphase fiber system and stacking sequence on low-velocity impact and residual tensile behavior of glass/epoxy composite laminates. *Polym Compos*. 2019;40(4):1450-1462. doi:10.1002/pc.24884

41. Sun X, Qu P, Liu G, Yi X, Su H, Jia Y. Analysis on low velocity impact damage of laminated composites toughened by structural toughening layer. *Polym Compos*. 2017;38(7):1280-1291. doi:10.1002/pc.23693

42. Hu D, Liu X, Liu W, Li G, Rudd C, Yi X. The effects of compaction and interleaving on through-thickness electrical resistance and in-plane mechanical properties for CFRP laminates. *Compos Sci Technol*. 2022;223(January):109441. doi:10.1016/j.compscitech.2022.109441

43. Yi XS, An XF. Effect of interleaf sequence on impact damage and residual strength in a graphite/epoxy laminate. *J Mater Sci*. 2004;39(9):3253-3255. doi:10.1023/B:JMSC.0000025872.39337.16

44. Riccio A, Russo A, Sellitto A, Raimondo A. Development and application of a numerical procedure for the simulation of the "fibre bridging" phenomenon in composite structures. *Compos Struct*. 2017;168:104-119. doi:10.1016/j.compstruct.2017.02.037

45. Suksangpanya N, Yaraghi NA, Pipes RB, Kisailus D, Zavattieri P. Crack twisting and toughening strategies in Bouligand architectures. *Int J Solids Struct*. 2018;150:83-106. doi:10.1016/j.ijsolstr.2018.06.004

46. Amorim L, Santos A, Nunes JP, Dias G, Viana JC. Quasi static mechanical study of vacuum bag infused bouligand inspired composites. *Polym Test*. 2021;100(December 2020):107261. doi:10.1016/j.polymertesting.2021.107261

47. Acanfora V, Sellitto A, Russo A, Zarrelli M, Riccio A. Experimental investigation on 3D printed lightweight sandwich structures for energy absorption aerospace applications. *Aerosp Sci Technol*. 2023;137:108276. doi:10.1016/j.ast.2023.108276

48. Acanfora V, Zarrelli M, Riccio A. Experimental and numerical assessment of the impact behaviour of a composite sandwich panel with a polymeric honeycomb core. *Int J Impact Eng*. 2023; 171(March 2022):104392. doi:10.1016/j.ijimpeng.2022.104392

49. Choi HY, Chang F. A model for predicting damage in graphite/epoxy laminated composites resulting from low-velocity point impact. *J Compos Mater*. 1992;26:2134-2169. doi:10.1177/002199839202601408

50. Lee SM, Zahuta P. Instrumented impact and static indentation of composites. *J Compos Mater*. 1991;25(2):204-222. doi:10.1177/002199839102500205

51. Wagih A, Maimí P, Blanco N, Costa J. A quasi-static indentation test to elucidate the sequence of damage events in low velocity impacts on composite laminates. *Compos Part A Appl Sci Manuf*. 2016;82:180-189. doi:10.1016/j.compositesa.2015.11.041

52. Belingardi G, Vadori R. Influence of the laminate thickness in low velocity impact behavior of composite material plate. *Compos Struct*. 2003;61(1–2):27-38. doi:10.1016/S0263-8223(03)00027-8

53. Quaresimin M, Ricotta M, Martello L, Mian S. Energy absorption in composite laminates under impact loading. *Compos Part B Eng*. 2013;44(1):133-140. doi:10.1016/j.compositesb.2012.06.020

54. Mehdikhani M, Gorbatikh L, Verpoest I, Lomov SV. Voids in fiber-reinforced polymer composites: a review on their formation, characteristics, and effects on mechanical performance. *J Compos Mater*. 2019;53(12):1579-1669. doi:10.1177/0021998318772152

55. Herráez M, González C, Lopes CS, et al. Computational micromechanics evaluation of the effect of fibre shape on the transverse strength of unidirectional composites: An approach to virtual materials design. *Compos Part A Appl Sci Manuf*. 2016; 91:484-492. doi:10.1016/j.compositesa.2016.02.026

56. Mohan J, Ivanković A, Murphy N. Mode i fracture toughness of co-cured and secondary bonded composite joints. *Int J Adhes Adhes*. 2014;51:13-22. doi:10.1016/j.ijadhadh.2014.02.008

SUPPORTING INFORMATION

Additional supporting information can be found online in the Supporting Information section at the end of this article.

How to cite this article: Amorim L, Santos A, Nunes JP, Dias G, Viana JC. A novel strategical approach to mitigate low velocity impact damage in composite laminates. *Polym Compos*. 2024;1-18. doi:10.1002/pc.28463